Unsupervised Fouling Reconstruction in the Pipe Bend

Denys Iablonskyi
Department of Computer Science, Department of Physics, University of Helsinki
Helsinki, Finland
denys.iablonskyi@helsinki.fi

Carlos-Omar Rasgado-Moreno
Department of Civil Engineering and Architecture, Tallinn University of Technology
Tallinn, Estonia
carlos.rasgado@taltech.ee

Madis Ratassepp
Department of Civil Engineering and Architecture, Tallinn University of Technology
Tallinn, Estonia
madis.ratassepp@taltech.ee

Arto Klami
Department of Computer Science University of Helsinki
Helsinki, Finland
arto.klami@helsinki.fi

Edward Hæggström
Department of Physics University of Helsinki
Helsinki, Finland
edward.haeggstrom@helsinki.fi

Ari Salmi
Department of Physics University of Helsinki
Helsinki, Finland
ari.salmi@helsinki.fi

***Abstract* — Guided wave tomography allows the investigation of extended areas with a limited number of measurements, typically using transducer arrays. Most imaging methods rely heavily on the material properties such as dispersion curves, that in the case of fouling deposition are not always known. In the case of complex shaped structures, geometrical anisotropy can bring additional complexity. Here we present an unsupervised machine learning approach based on the Gaussian process to detect and characterize the fouling in a pipe bend that relies only on the difference between clean/healthy and fouled/damaged measured signals.**

Keywords — guided waves, structural health monitoring, non-destructive testing, fouling detection, Gaussian processes

I. Introduction

Pipes can become fouled for several reasons when unwanted substances accumulate on their inner surfaces. These substances can include mineral deposits, sediment, biological matter, corrosion, and chemical deposits. Detection and characterization of the fouled area are thus of critical importance for efficient industrial operations [1]. It has been shown that Lamb waves, typically generated using a network of ultrasonic transducers, are sensitive to most fouling materials and defects. Several algorithms were proposed to reconstruct fouling/flaw map inside the pipe-like structures based on the attenuation of the propagating waves [2], the variation in the wave velocity [3,4], and the changes in the time-of-arrival of the wave packets [5]. These methods rely on the accurate attenuation data or simulated dispersion curves that are not always known in case of an unknown fouling material. Recently we proposed unsupervised machine learning approach *i.e.*, Gaussian process, to detect and characterize the fouling in a pipe based on changes in the measured signals [6]. In this paper we apply this reconstruction algorithm to experimental data obtained from a pipe bend. In contrast to other tomographic methods, our approach does not require information about the structure or the fouling materials, but instead only requires the measurements made with and without fouling.

II. Experiment

The experimental setup is shown in Fig. 1. A steel pipe bend is 21.9 cm in diameter with 8 mm wall thickness. The bend has a curvature radius of 32.9 cm and a bending angle of 90°. Two rings of transducers are located at each end of the bend. Each ring consists of 20 piezoelectric transducers with a central frequency of 50 kHz evenly placed along the circumference. They can be used as both transducers and receivers. For data acquisition we used National Instruments USB-6349 that has a sampling rate of 500 kS/s with 16-bit ADC resolution. Detailed description of the pipe bend, transducers, and the acquisition system can be found in [7]. Each of the transducers in the left ring was sequentially excited with 3 cycles at 60 kHz and all transducers in the right ring recorded the transmitted signal, resulting in 400 recorded signals. The measurement was conducted on an empty pipe bend as a reference. Then the plasticine of about 10 cm diameter was attached on top of the bend to resemble fouling effect and the measurement was repeated (see Fig. 1).

The amplitudes of the first arriving A_0 Lamb-like mode that corresponds to the shortest path were extracted using calculated time-of-arrival (TOA) for each receiving transducer using the continuous wavelet transform (CWT). It was found during the analysis that the CWT is much more resilient to noise and low sampling ratio than the Hilbert transform and thus provides more accurate amplitude retrieval. The resulting attenuation ratios due to the fouling were calculated as A^{empty}/A^{foul} and are depicted in Fig. 1. To not rely on any attenuation model, we further simplified the input to reconstruction method by truncating the attenuation ratios to be ether 0 or 1 by setting a certain threshold *e.g.,* 0.97. Thus, when the signal amplitude decreased by more than 3%, we set the model input to 1 *i.e.*, the traveled wave crossed through some fouling along the way for a certain pair of transducers. When the decrease in amplitude is less than 3%, the wave did not intersect any fouling.

III. Reconstruction Method

The fouling reconstruction is formulated as a probabilistic modeling problem, where the 2D fouling map on the pipe bend surface was assumed to be smoothly varying non-negative function that follows a Gaussian process (GP) prior with zero mean and a covariance function K:

$$f(x,y) \sim GP\big(0, K(x,y;x',y')\big). \quad (1)$$

Generally, the GP prior is a collection of random functions, thus, the task is to find a GP posterior distribution conditional on the experimental observation *i.e.*, to generate random fouling maps from the prior distribution and reject all

This work was supported by the Research Council of Finland (project codes 324852, 336019, 336020, 353441) and the Estonian Research Council (grant PRG737).

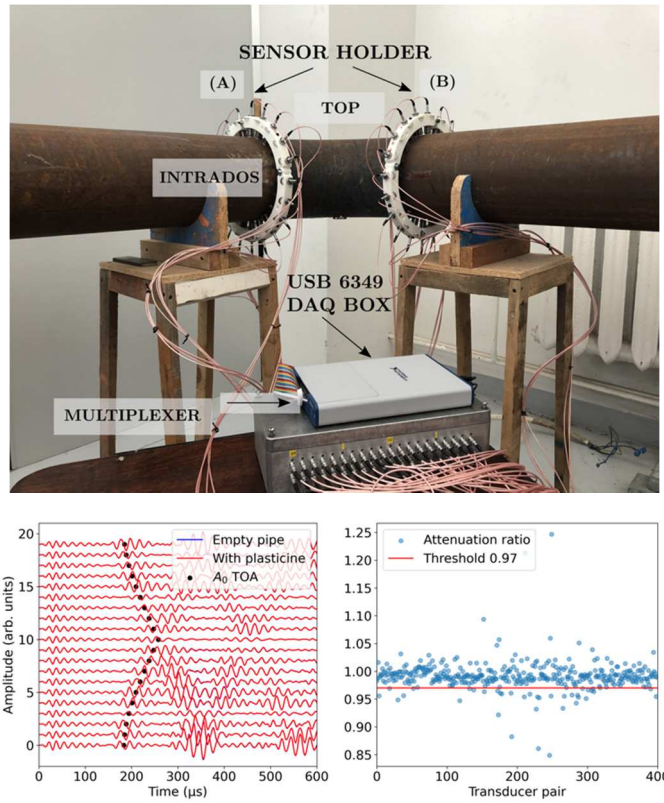

Fig. 1. Experimental setup (upper). Recorded signals with the right transducer ring when the inner transducer in the left ring is excited (lower left). Extracted attenuation ratios of the A_0 Lamb mode (lower right).

that do not agree with the observations [8]. The covariance function consists of squared exponential kernel along the x-axis and a circumferential periodicity along y-axis is encoded using an exponentiated sine kernel.

The binary classification observations $y_n = \{0,1\}$ *i.e.*, whether the signal between the pair of transducers n travels through the fouling or not, was then modeled using the discrete Bernoulli distribution of the inverse logistic transformation of the integrated fouling map:

$$y_n \sim Bernoulli\left(logit^{-1}(F_n + c)\right), \tag{2}$$

where c is the bias term to correct imbalanced classes in the training data, F_n is the integral of the fouling along the trajectory between the pair of transducers:

$$F_n = \int_{trajectory} S(f(x,y) - h)dxdy. \tag{3}$$

Here $S(\bullet)$ is the sigmoid transformation that enforces fouling non-negativity proposed in [9] and maps it to $[0,1]$, h is the constant that controls the expected fouling probability. Constants c and h are unknown and are inferred from the data together with the model parameters.

For practical computation of (3) we consider a finite set of pixels $(G_x, G_y) = (35,35)$ along the x and y axes of the unraveled pipe bend. Each pixel size corresponds to 2 cm on the pipe bend. The integral is then transformed into matrix multiplication of the trajectory map and the fouling map. Due to the bend structure, the shortest trajectory between the pair

Fig. 2. The shortest trajectory between the top transducer in the left ring and every 4th transducer in the right ring. The 2D image of the pipe bend is obtained by unraveling the 3D pipe bend along the bend's inner line (intrados in Fig. 1). The transducer rings are located along the left and right sides of the images.

of transducers in the opposite rings is not along the straight lines as in the case of straight pipes and the geodesic equations need to be solved to obtain the shortest path trajectory. It is a one-time operation that only needs to be solved for the specific geometry once and hence can be done with the direct numerical computation. An example of the trajectory maps between transducer at the top of the left ring and every 4th transducer in the opposite ring is shown in Fig. 2. The integral in (3) can be written as:

$$F_n = \boldsymbol{T}_n S(\boldsymbol{f} - h), \tag{4}$$

where $\boldsymbol{T}_n$ is the trajectory binary matrix for each pair of transducers n, $\boldsymbol{f}$ is the fouling matrix.

The posterior inference of the fouling map was performed using No U-Turn Sampler (NUTS) in the probabilistic programing language *Stan* [10]. In addition, we performed inference of the model hyperparameters c and h. The covariance function used fixed characteristic length scales along the x and y axes equal to 4 pixels that corresponds to 8 cm on the pipe bend. A more detailed description of the reconstruction method in case of straight pipe is presented in [6, 9].

IV. Results

As one can see from the recorded wave signals in Fig. 1 when the transducer on the inner side of the bend is excited, the signal recorded signal by the 11th transducer on the outside of the bend was substantially reduced. Due to cylindrical structure of the pipe bend some of the wave packets that propagate clockwise and anticlockwise can overlap at the receiving transducers which causes unwanted interference. Thus, the attenuation information cannot be extracted reliably. Overall, 24 observations out of the 400 were omitted in the reconstruction analysis. As mentioned in Sec. II, the experimental attenuation ratios were truncated to binary values $y_n = \{0,1\}$ using some attenuation threshold value (*e.g.*, 3%). This allowed us to avoid using an attenuation model in the reconstruction algorithm as well as reduces the experimental efforts.

Posterior inference of the unknown fouling map using sampling results in a distribution over the different fouling maps that follow the same Gaussian process. This allowed us to calculate the mean and the standard deviation of the fouling map depicted in Fig. 3. The reconstructed fouling map agrees reasonably well with the position of the plasticine loading of about 10cm diameter (on top of the bend). Due to rather little attenuation of the signal that propagated through the fouled area (3% threshold was selected empirically), there could be some false positive labels that led to a few fouling spots located near the transducer rings (left and right sides of the image in Fig. 3). Increasing the attenuation threshold did not

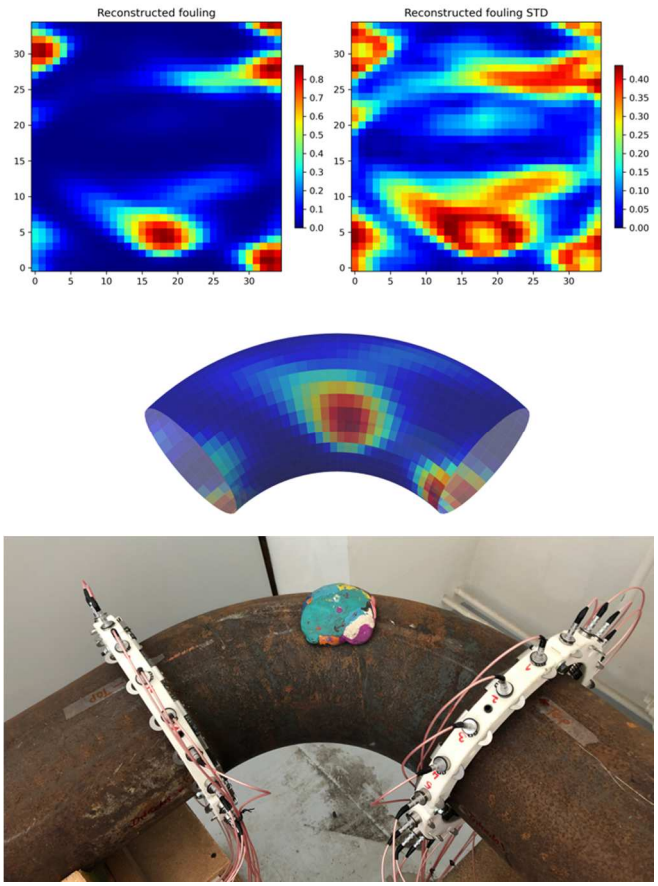

Fig. 3. The mean and the standard deviation of the fouling map reconstruction distribution on the unraveled pipe bend (upper row). 3D visualization of the fouling map (middle). The round plasticine patch of 10 cm diameter was placed on top of the pipe bend (lower).

improve the reconstruction of the fouling map. One reason for the low attenuation could be weak adhesion of the plasticine patch to the rusty steel pipe bend. As seen in Fig. 1, some of the attenuation ratios are above 1, that indicates experimental challenges in collecting robust data. The standard deviation of the extracted ratios is 2.7% indicating robust fouling reconstruction by the proposed method in this challenging experimental environment. Possible improvements to the fouling reconstruction can be made by utilizing higher order helical trajectories, since in the current study only amplitudes of the first arriving A_0 modes were used.

V. Conclusions

We presented experimental verification of the fouling reconstruction method in a pipe bend based on the binary classification formulation of the Gaussian process. The shape and location of the fouling phantom (*e.g.*, plasticine) was reconstructed reasonably well within the standard deviation despite noisy experimental observations. Experimental challenges were discussed, and possible improvements were proposed.

References

[1] K. R. Lohr and J. L. Rose, “Ultrasonic guided wave and acoustic impact methods for pipe fouling detection,” J Food Eng 56, 4, pp. 315-324 (2003).

[2] K. R. Leonard and M. K. Hinders, “Lamb wave tomography of pipe-like structures,” Ultrasonics 43, pp. 574–583 (2005).

[3] P. Huthwaite and F. Simonetti, “High-resolution guided wave tomography,” Wave Motion 50, 979–993 (2013).

[4] J. Rao, M. Ratassepp and Z. Fan, "Guided Wave Tomography Based on Full Waveform Inversion," IEEE Transactions on Ultrasonics, Ferroelectrics, and Frequency Control 63, 5, pp. 737-745 (2016)

[5] T. Sillanpää, T. Rauhala, J. Mäkinen, C. Rajani, K. Longi, A. Klami, A. Salmi, and Edward Hæggström, “Ultrasonic fouling detector powered by machine learning,” 2019 IEEE International Ultrasonics Symposium (IUS), 1639-1642 (2019).

[6] D. Iablonskyi, H. Wei, A. Klami, A. Salmi, and E. Hæggström, "Reconstruction of Fouling Distribution from Aggregate Observations," 2022 IEEE International Ultrasonics Symposium (IUS), pp. 1-4 (2022).

[7] C.-O. Rasgado-Moreno, M. Rist, R. Land, and M. Ratassepp, “Acoustic Forward Model for Guided Wave Propagation and Scattering in a Pipe Bend,” Sensors 22, 2, p. 486 (2022).

[8] C. E. Rasmussen and C. K. I. Williams, “Gaussian Processes for Machine Learning,” MIT Press (2006).

[9] V. Tanskanen, K. Longi, and A. Klami, "Non-Linearities in Gaussian Processes with Integral Observations," 2020 IEEE 30th International Workshop on Machine Learning for Signal Processing (MLSP), 1-6 (2020).

[10] B. Carpenter, A. Gelman, M. Hoffman, D. Lee, B. Goodrich, M. Betancourt, M. Brubaker, J. Guo, P. Li, and A. Riddell, “Stan: A Probabilistic Programming Language,” Journal of Statistical Software, 76(1), 1–32 (2017).